

## Supporting Information

### Insights into the Electrochemical Catalytic Mechanism of Atomically Dispersed Metal on h-BCN Monolayer

Na Zhou <sup>a</sup>, Yanning Wang <sup>\*,b</sup>, Jiao Wang <sup>a</sup>, Panchao Zhao <sup>a</sup>, Hang Zhang <sup>b</sup>

<sup>a</sup> Northwest Institute for Non-Ferrous Metal Research, Xi'an, Shaanxi 710016, China

<sup>b</sup> National Key Laboratory of Aerospace Flight Technology, Beijing Aerospace Technology Research Institute, Beijing 100074, China

---

\*Corresponding author.

E-mail address: [wwangyanning@163.com](mailto:wwangyanning@163.com)

## 1. Computational details

The Gibbs free energy ( $\Delta G$ ) for the ORR/OER of each step is defined as

$$\Delta G = \Delta E + \Delta E_{ZPE} - T\Delta S \quad (\text{S1})$$

where  $\Delta E$  is the adsorption energy of the catalytic intermediates on M-SACs@h-BCN.  $\Delta E_{ZPE}$  is the zero-point energy.  $\Delta S$  is the entropy difference between the adsorbed state and the free-standing state.  $T$  is the reaction temperature ( $T = 298.15$  K) [S1].

The equations of free energy changes are [S2]

$$\Delta G_1 = \mu_{OOH^*} + \mu_{OH^-} - \mu_{O_2(g)} - \mu_{H_2O(l)} - \mu_e^- - \mu_* = \Delta G_{OOH^*} - 4.92 + eU \quad (\text{S2a})$$

$$\Delta G_2 = \mu_{O^*} + \mu_{OH^-} - \mu_{OOH^*} - \mu_e^- = \Delta G_{O^*} - \Delta G_{OOH^*} + eU \quad (\text{S2b})$$

$$\Delta G_3 = \mu_{OH^*} + \mu_{OH^-} - \mu_{O^*} - \mu_{H_2O(l)} - \mu_e^- = \Delta G_{OH^*} - \Delta G_{O^*} + eU \quad (\text{S2c})$$

$$\Delta G_4 = \mu_{OH^-} + \mu_* - \mu_{OH^*} - \mu_e^- = -\Delta G_{OH^*} + eU \quad (\text{S2d})$$

where

$$\Delta G_{OOH^*} = \mu_{OOH^*} + \frac{3}{2} \mu_{H_2(g)} - 2\mu_{H_2O(l)} - \mu_* \quad (\text{S3a})$$

$$\Delta G_{O^*} = \mu_{O^*} + \mu_{H_2(g)} - \mu_{H_2O(l)} - \mu_* \quad (\text{S3b})$$

$$\Delta G_{OH^*} = \mu_{OH^*} + \frac{1}{2} \mu_{H_2(g)} - \mu_{H_2O(l)} - \mu_* \quad (\text{S3c})$$

## 2. Figures

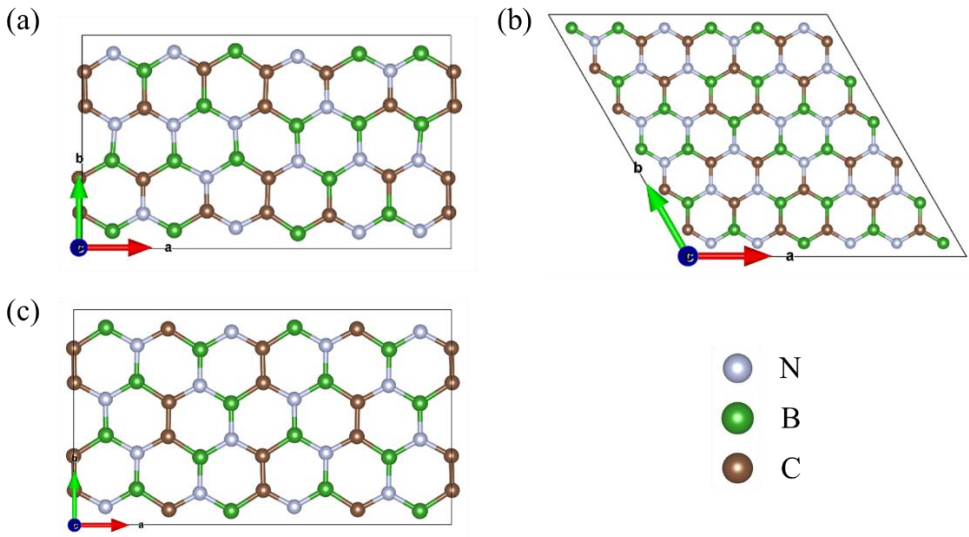


Figure S1. Optimized structures of three plausible h-BCN monolayers. (a) BCN\_V1 with  $a = 15.12 \text{ \AA}$  and  $b = 8.73 \text{ \AA}$ . (b) BCN\_V2 with  $a = 15.13 \text{ \AA}$  and  $b = 15.13 \text{ \AA}$ . (c) BCN\_V3 with  $a = 15.19 \text{ \AA}$  and  $b = 8.65 \text{ \AA}$ .

Three plausible h-BCN monolayer structures [S3, S4], including BCN\_V1, BCN\_V2 and BCN\_V3, are constructed, as shown in Figure S1. All the structures present similar structures of graphene. The optimized lattice parameters for the three structures are shown in Table S1. All of the lattice parameters are in good agreement with previous results [S3, S4]. The unit energies, which consisted by the energy of a single boron, carbon, and nitrogen atom, in BCN\_V1, BCN\_V2 and BCN\_V3 are -25.40 eV, -25.12 eV, and -25.79 eV, respectively. The BCN\_V3 is applied to be the study object in the present work due to its lowest energy and highest structural stability.

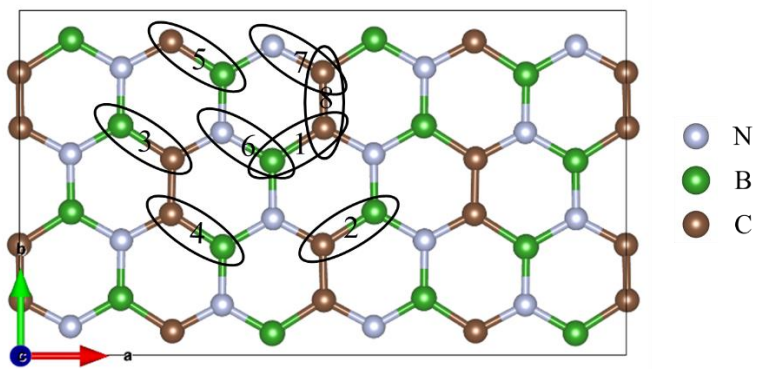


Figure S2. The possible vacancies by removing two adjacent atoms.

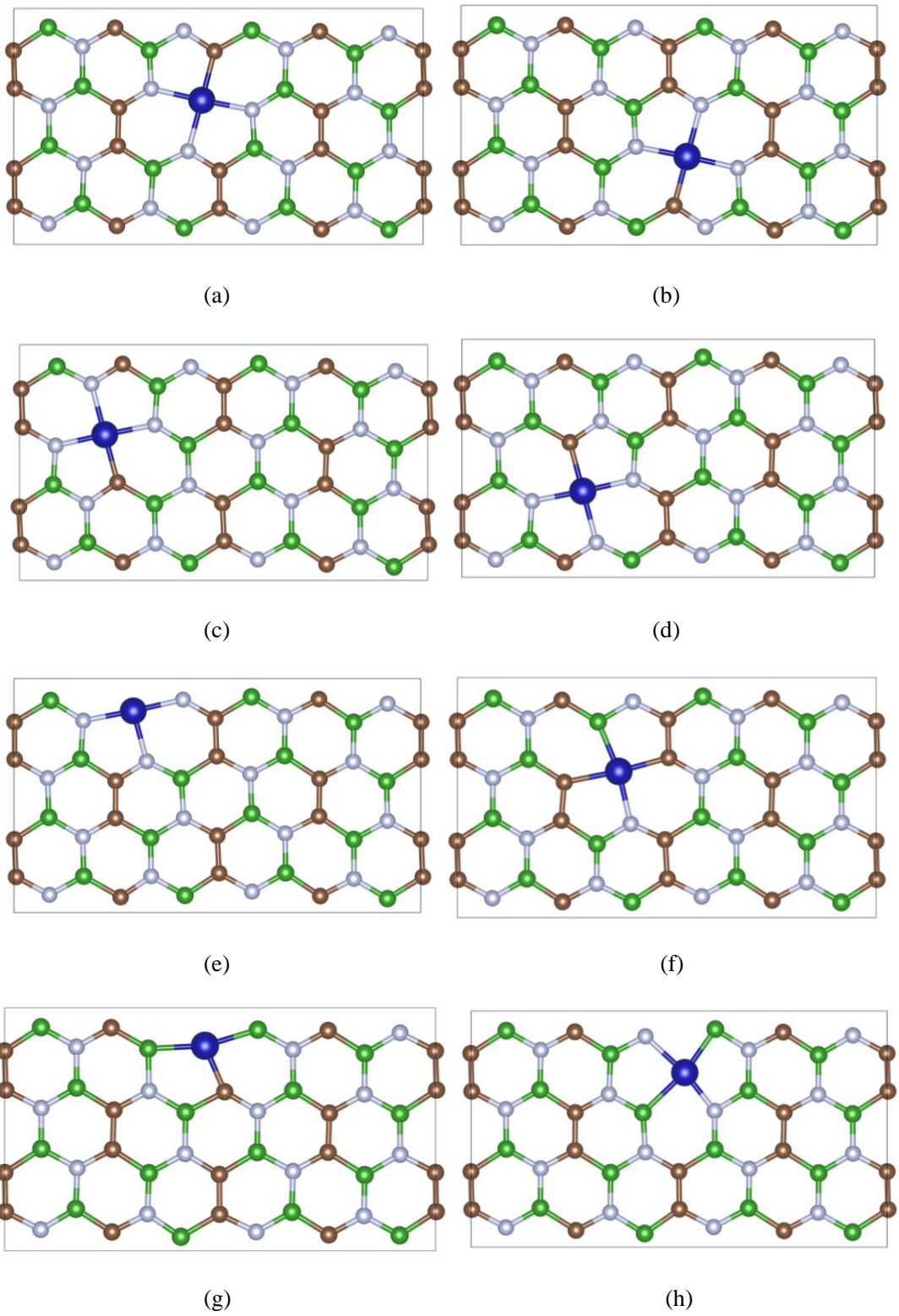


Figure S3. Multiple structures of Co single-atom catalysts (Co-SACs@h-BCN) formed by Co single atoms embedded in different sites of h-BCN monolayer. (a) Co-SACs@h-BCN-1. (b) Co-SACs@h-BCN-2. (c) Co-SACs@h-BCN-3. (d) Co-SACs@h-BCN-4. (e) Co-SACs@h-BCN-5. (f) Co-SACs@h-BCN-6. (g) Co-SACs@h-BCN-7. (h) Co-SACs@h-BCN-8.

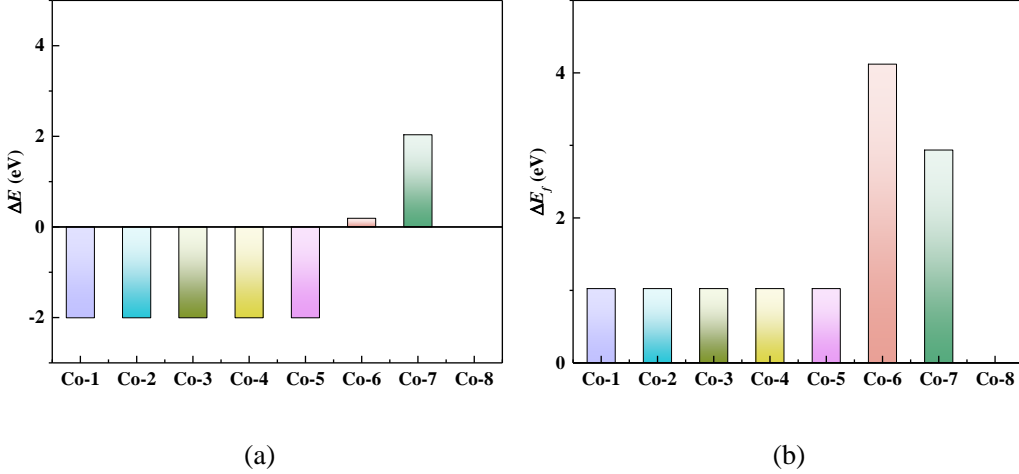


Figure S4. (a) Relative energy and relative formation energy ( $\Delta E_f$ ) of Co-SACs@h-BCN (Co-SACs@h-BCN-1, Co-SACs@h-BCN-2, Co-SACs@h-BCN-3, Co-SACs@h-BCN-4, Co-SACs@h-BCN-5, Co-SACs@h-BCN-6, Co-SACs@h-BCN-7 and Co-SACs@h-BCN-8) comparing with the Co-SACs@h-BCN-8.

To estimate the structure stabilities of different structures of Co-SACs@h-BCN, the formation energy  $E_f$  is defined as

$$E_f = E_{\text{TM-SACs@h-BCN}} + x\mu_B + y\mu_C + z\mu_N - E_{\text{h-BCN}} - \mu_{\text{TM}} \quad (\text{S4})$$

where  $E$  is the total energy obtained by DFT calculation,  $\mu$  is the chemical potential, the  $x$ ,  $y$  and  $z$  are the number of removed atoms, the subscript is the corresponding structure. For the h-BCN monolayer, two adjacent atoms are removed, resulting in that

$$x + y + z = 2 \quad (\text{S5})$$

The chemical potentials of B, C, and N atoms are derived from the total energy of borophene, graphene and nitrogen molecules.

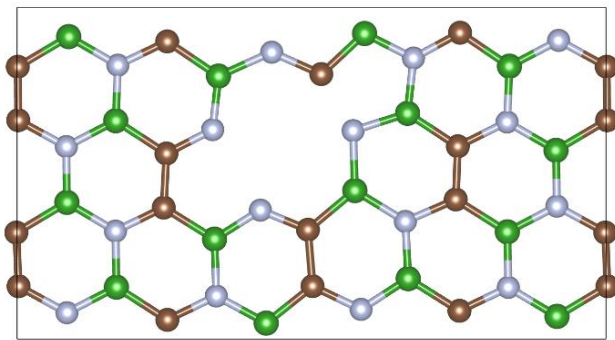
For ease of comparison, the relative energy ( $\Delta E$ ) and relative formation energy ( $\Delta E_f$ ) of Co-SACs@h-BCN compared with the Co-SACs@h-BCN-8 is defined as

$$\Delta E = E(\text{Co-SACs@h-BCN}) - E(\text{Co-SACs@h-BCN-8}) \quad (\text{S6})$$

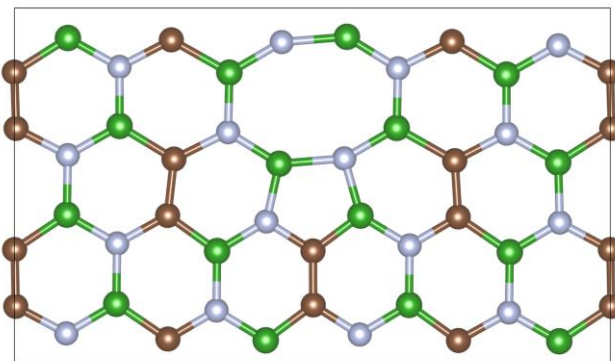
$$\Delta E_f = E_f(\text{Co-SACs@h-BCN}) - E_f(\text{Co-SACs@h-BCN-8}) \quad (\text{S7})$$

The calculation results are shown in Figure S4 and Table S2, it could be seen that the Co-SACs@h-BCN-1 shows the lowest energies while the Co-SACs@h-BCN-8

shows the lowest formation energies. The h-BCN monolayers with diatomic vacancy for the formation of Co-SACs@h-BCN-1 and Co-SACs@h-BCN-8 are shown in Figure S5. It could be seen that the vacancy for the formation of Co-SACs@h-BCN-1 is stable. However, the atomic reconstruction appears and the vacancy for the formation of Co-SACs@h-BCN-8 is unstable, going against the accommodation of a TM atom. The Co-SACs@h-BCN-1 are selected as the object in the following investigations.

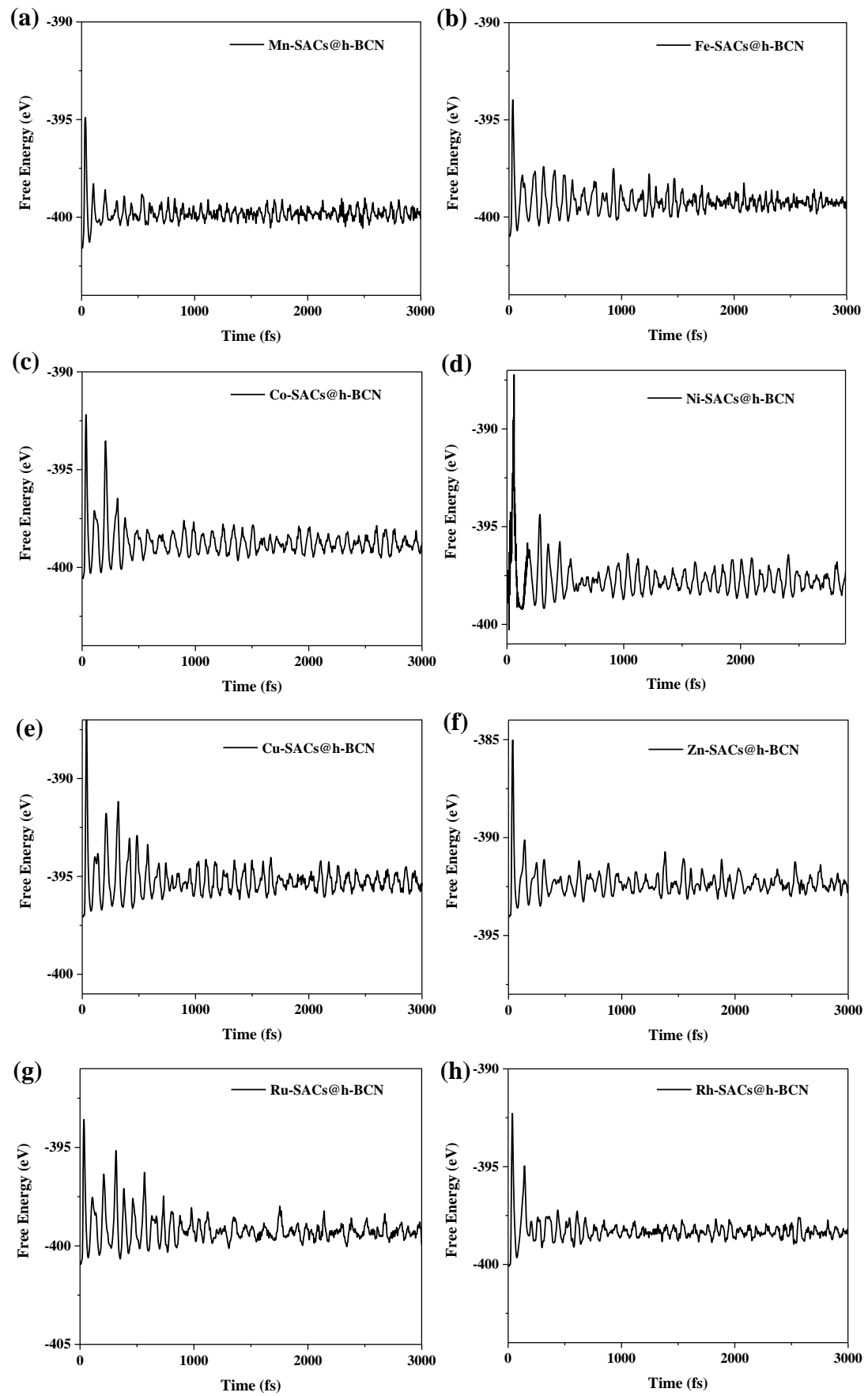


(a)



(b)

Figure S5. The h-BCN monolayer with diatomic vacancy. (a) Vacancy for the formation of Co-SACs@h-BCN-1. (b) Vacancy for the formation of Co-SACs@h-BCN-8.



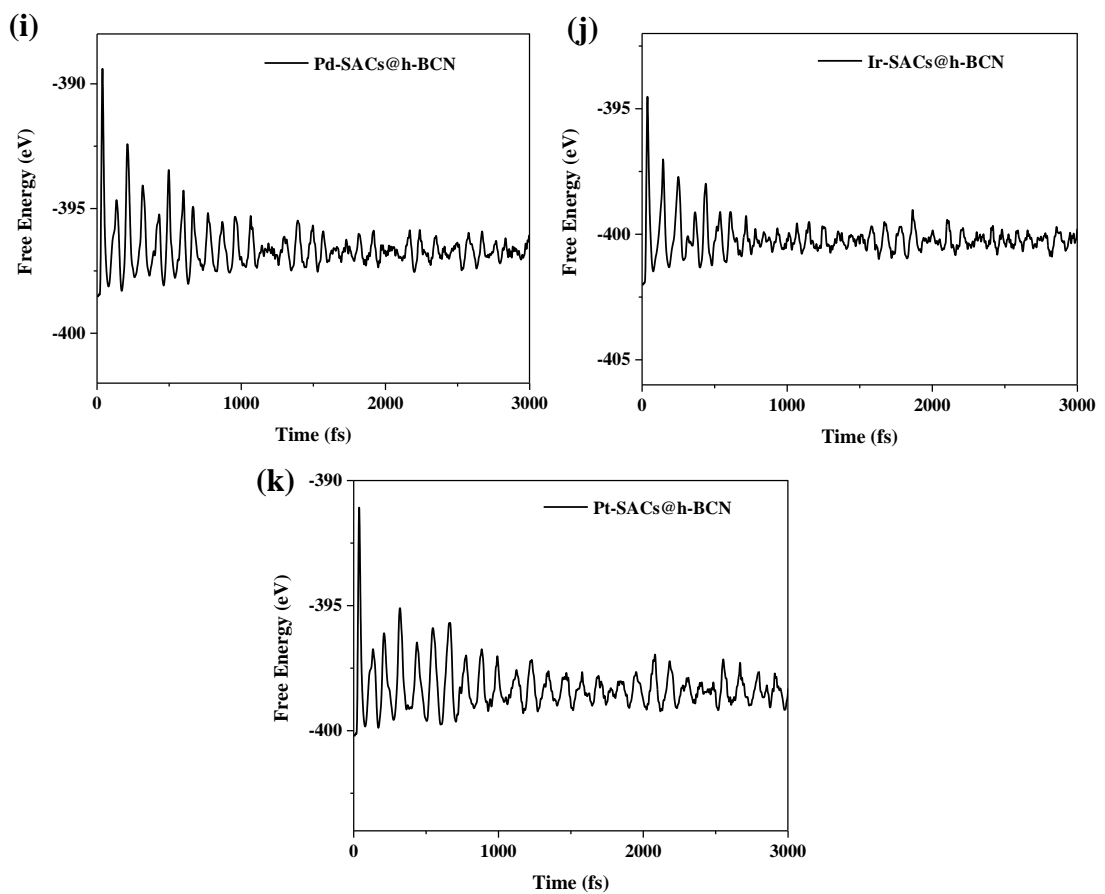


Figure S6. Free energy variations of M-N<sub>3</sub> embedded in h-BCN monolayer for AIMD simulations at 300 K. (a) Mn, (b) Fe, (c) Co, (d) Ni, (e) Cu, (f) Zn, (g) Ru, (h) Rh, (i) Pd, (j) Ir, (k) Pt.

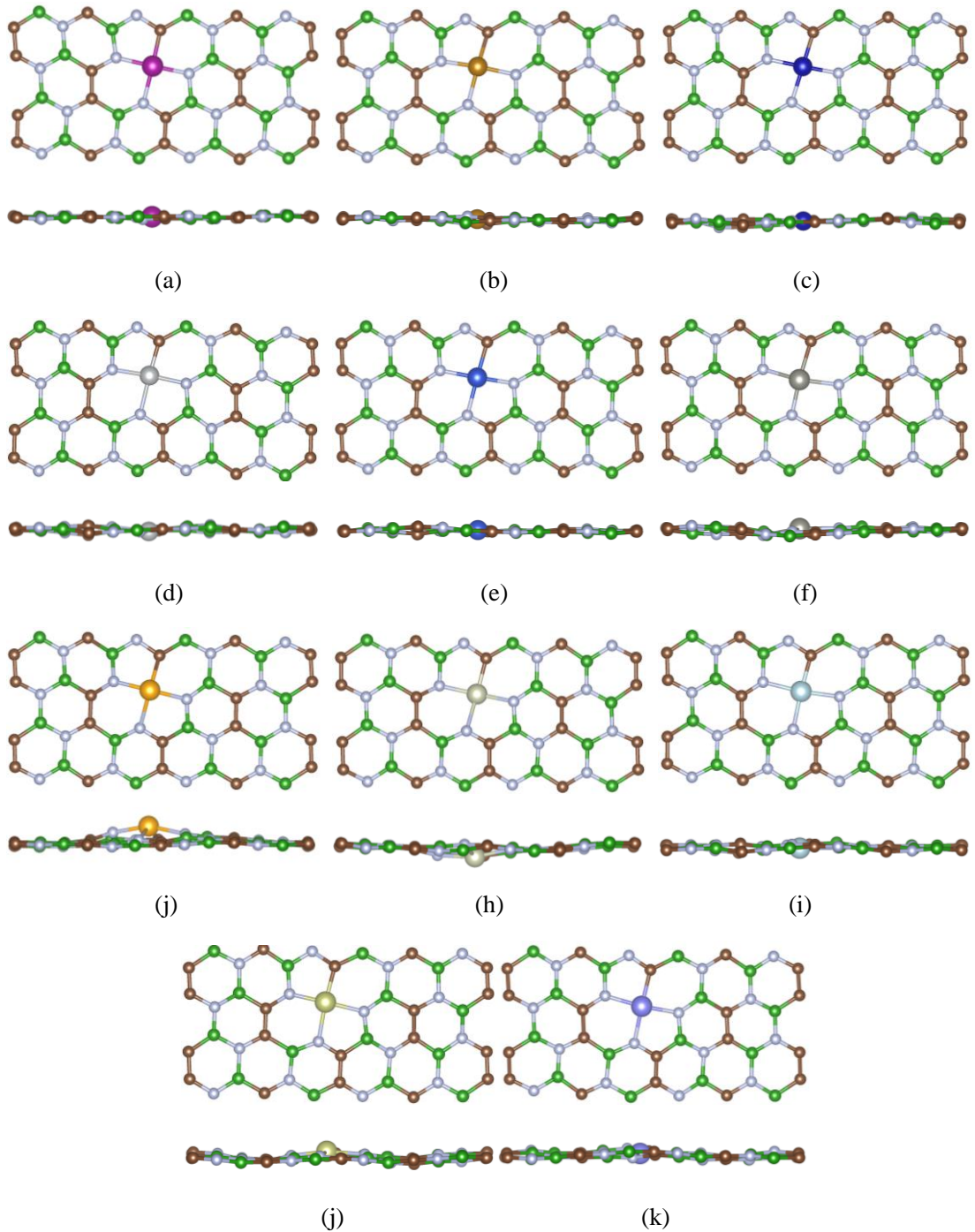


Figure S7. The top- and side-view structures of M-N<sub>3</sub> embedded in the h-BCN monolayer for AIMD simulations performed at 3000 fs. (a) Mn, (b) Fe, (c) Co, (d) Ni, (e) Cu, (f) Zn, (g) Ru, (h) Rh, (i) Pd, (j) Ir, (k) Pt.

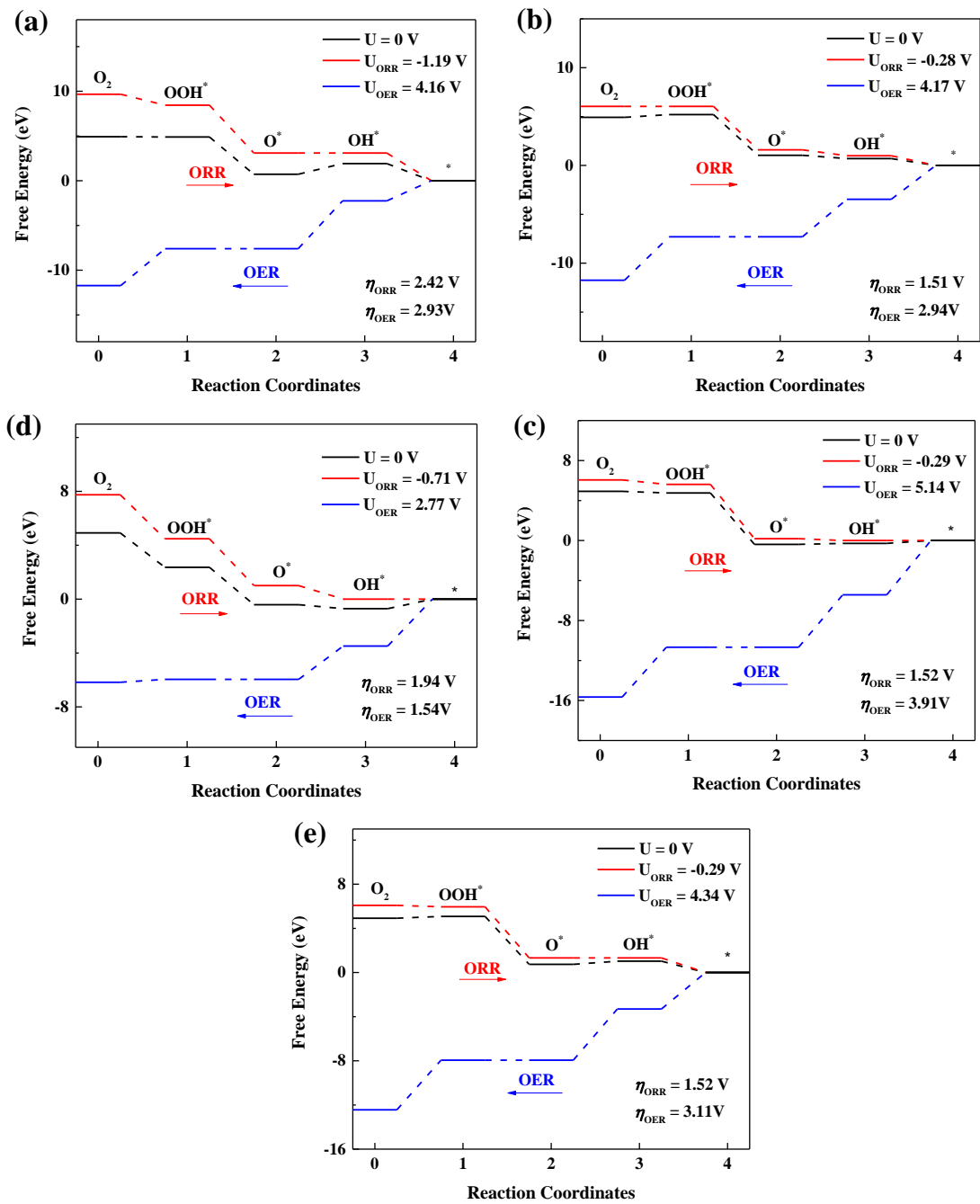


Figure S8. Free energy profiles of ORR and OER on (a) Ni-N<sub>3</sub>, (b) Cu-N<sub>3</sub>, (c) Zn-N<sub>3</sub>, (d) Ru-N<sub>3</sub> and (e) Pd-N<sub>3</sub> active sites.

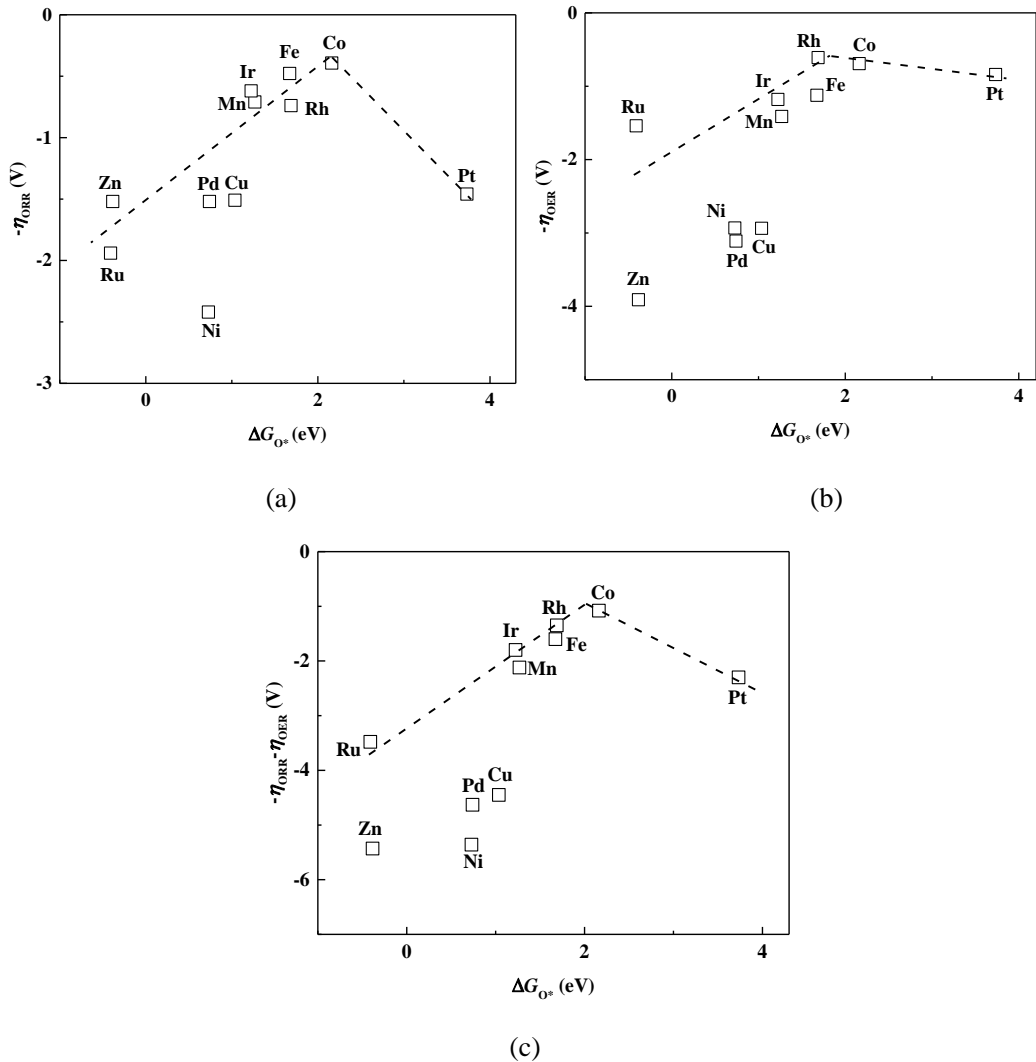


Figure S9. The overpotentials of ORR and OER against  $\Delta G_{O^*}$ . (a) Variation of  $-\eta_{ORR}$  against  $\Delta G_{O^*}$ . (b) Variation of  $-\eta_{OER}$  against  $\Delta G_{O^*}$ . (c) Variation of  $-\eta_{ORR} - \eta_{OER}$  against  $\Delta G_{O^*}$ .

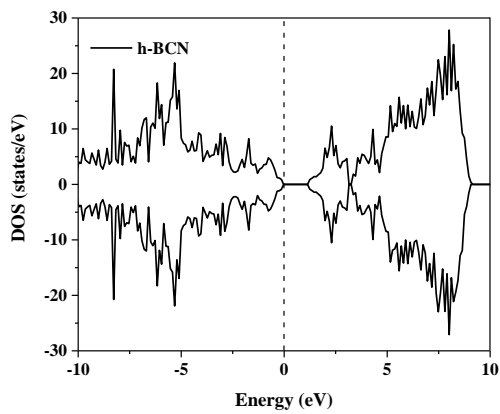
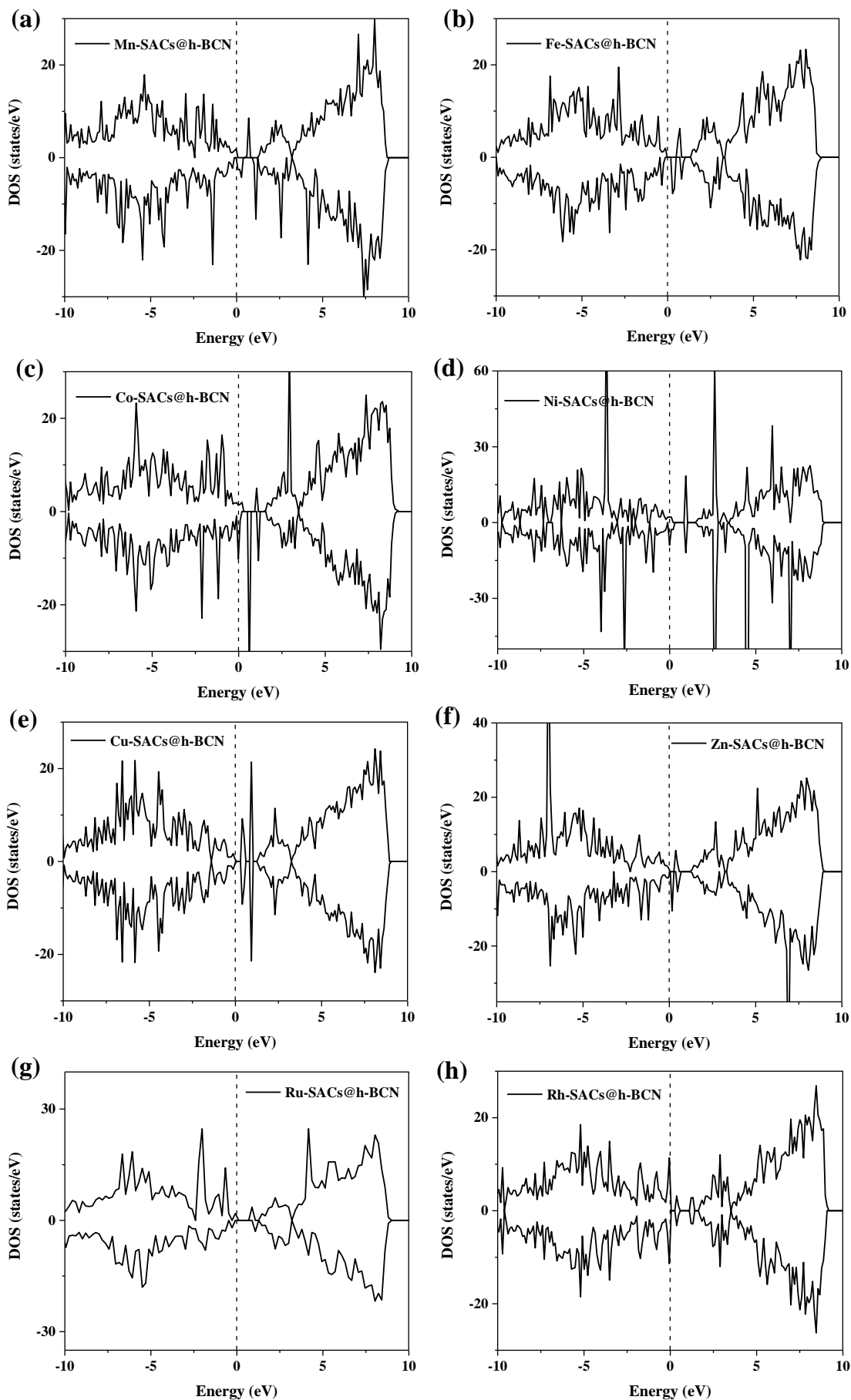


Figure S10. Density of states (DOS) curves for h-BCN monolayer. The Fermi energy level is 0 eV, labeled by the dashed line.



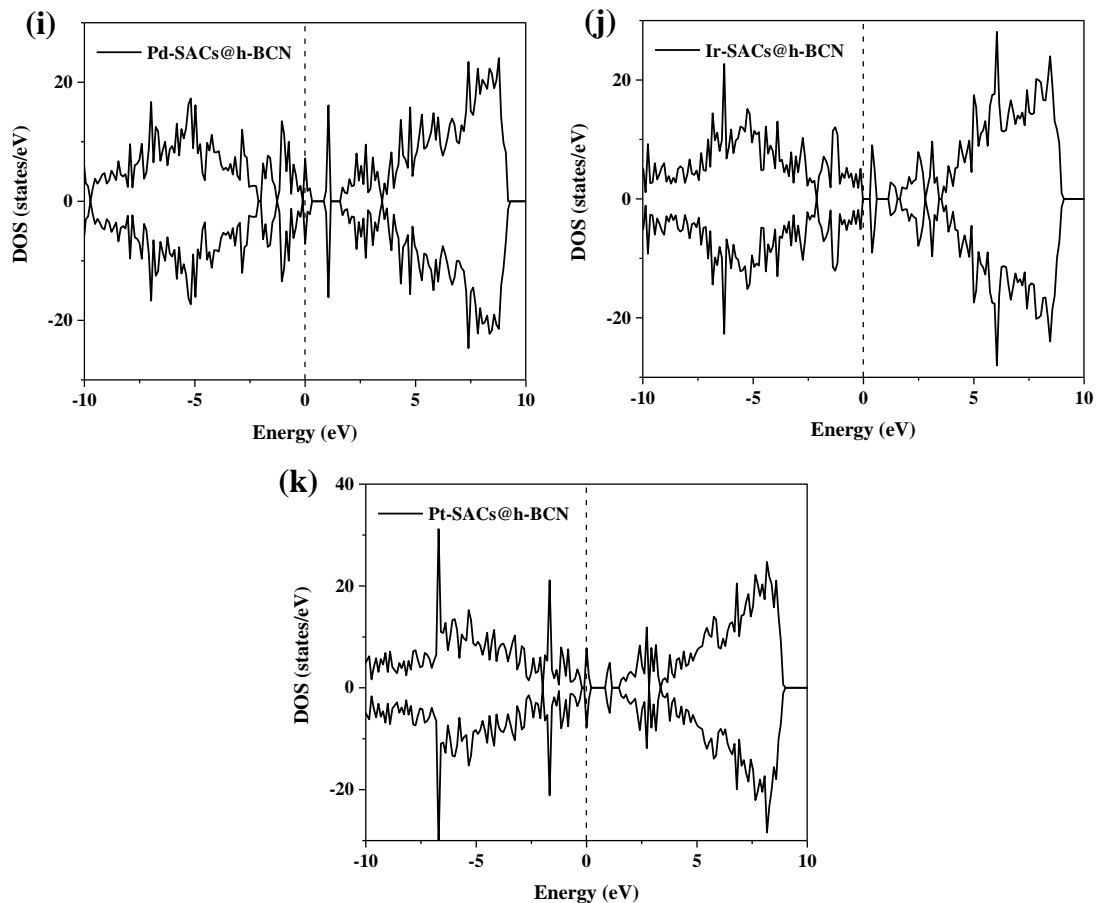


Figure S11. Density of states (DOS) curves of the M-SACs@h-BCN. The Fermi energy level is 0 eV, labeled by the dashed line.

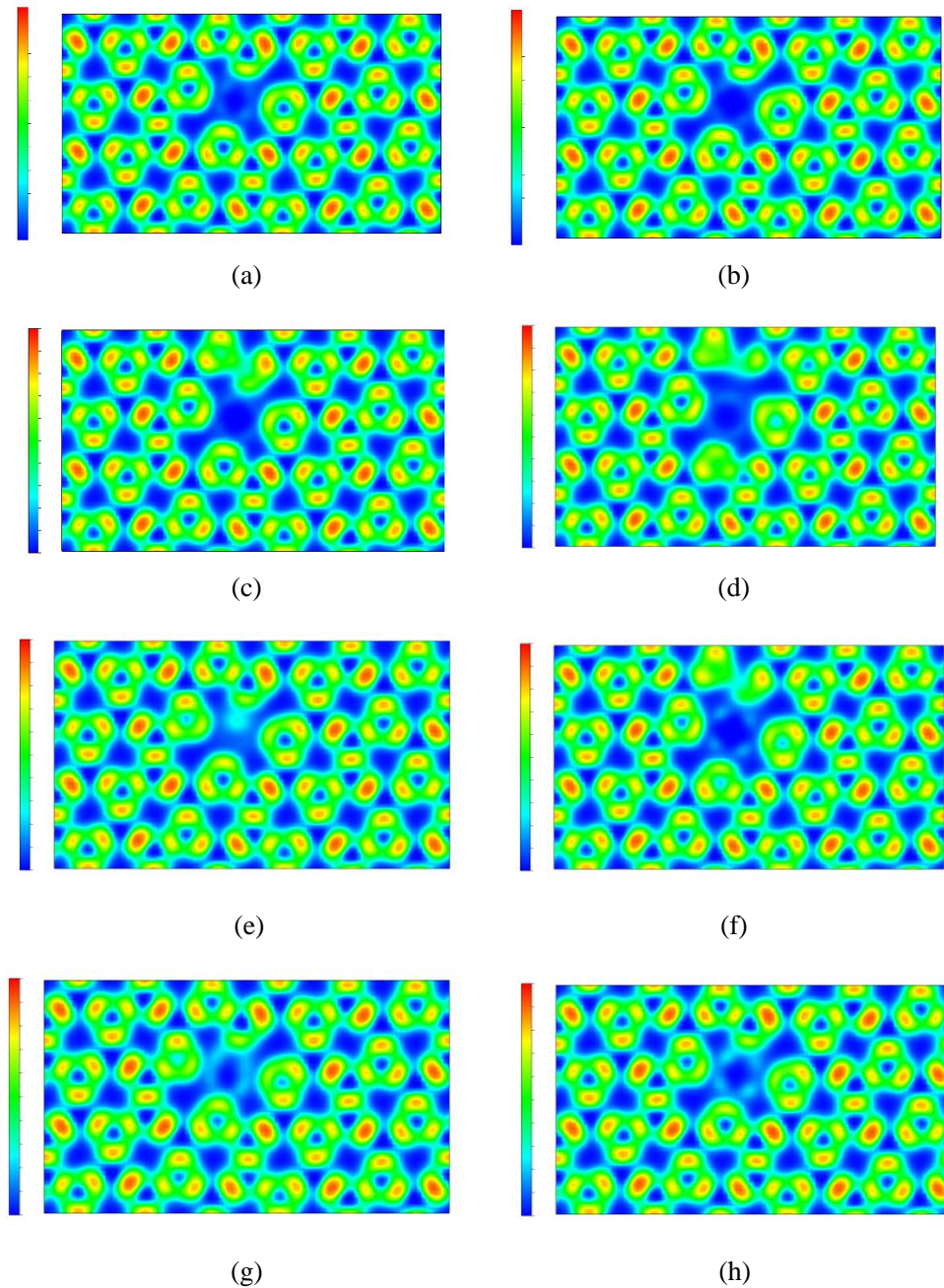


Figure S12. The electron localization function of M-SACs@h-BCN in the (001) plane with the OH adsorbed. (a) Mn-SACs@h-BCN, (b) Ni-SACs@h-BCN, (c) Cu-SACs@h-BCN, (d) Zn-SACs@h-BCN, (e) Ru-SACs@h-BCN, (f) Pd-SACs@h-BCN, (g) Ir-SACs@h-BCN, (h) Pt-SACs@h-BCN. The electron localization function contours are color-coded between 0.4 (blue) and 0.6 (red).

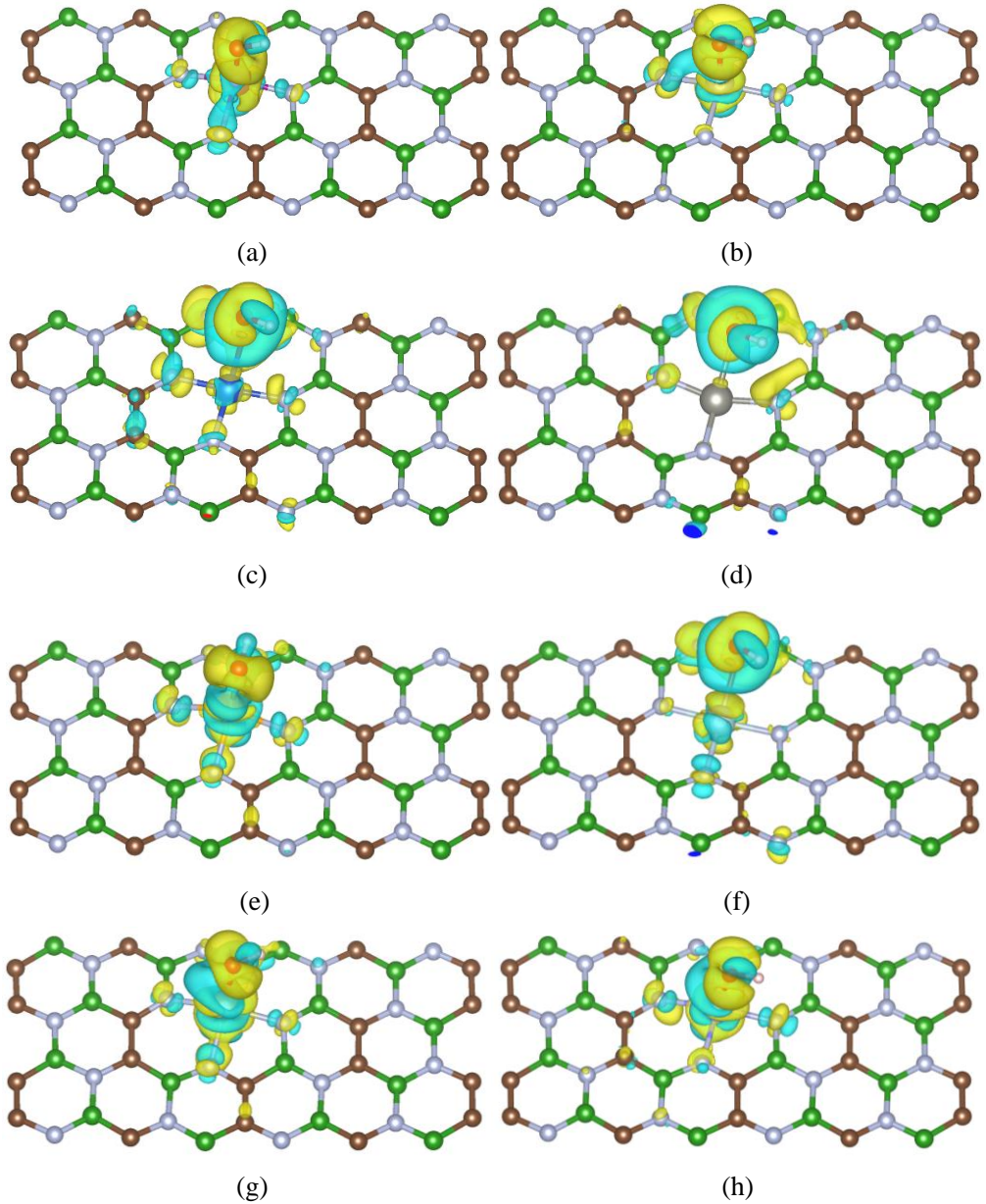


Figure S13. Charge difference plots of OH adsorbed on the M-N<sub>3</sub> active sites. The yellow and blue regions correspond to the charge sufficient area and deficient area, respectively. (a) Mn-SACs@h-BCN, (b) Ni-SACs@h-BCN, (c) Cu-SACs@h-BCN, (d) Zn-SACs@h-BCN, (e) Ru-SACs@h-BCN, (f) Pd-SACs@h-BCN, (g) Ir-SACs@h-BCN, (h) Pt-SACs@h-BCN.

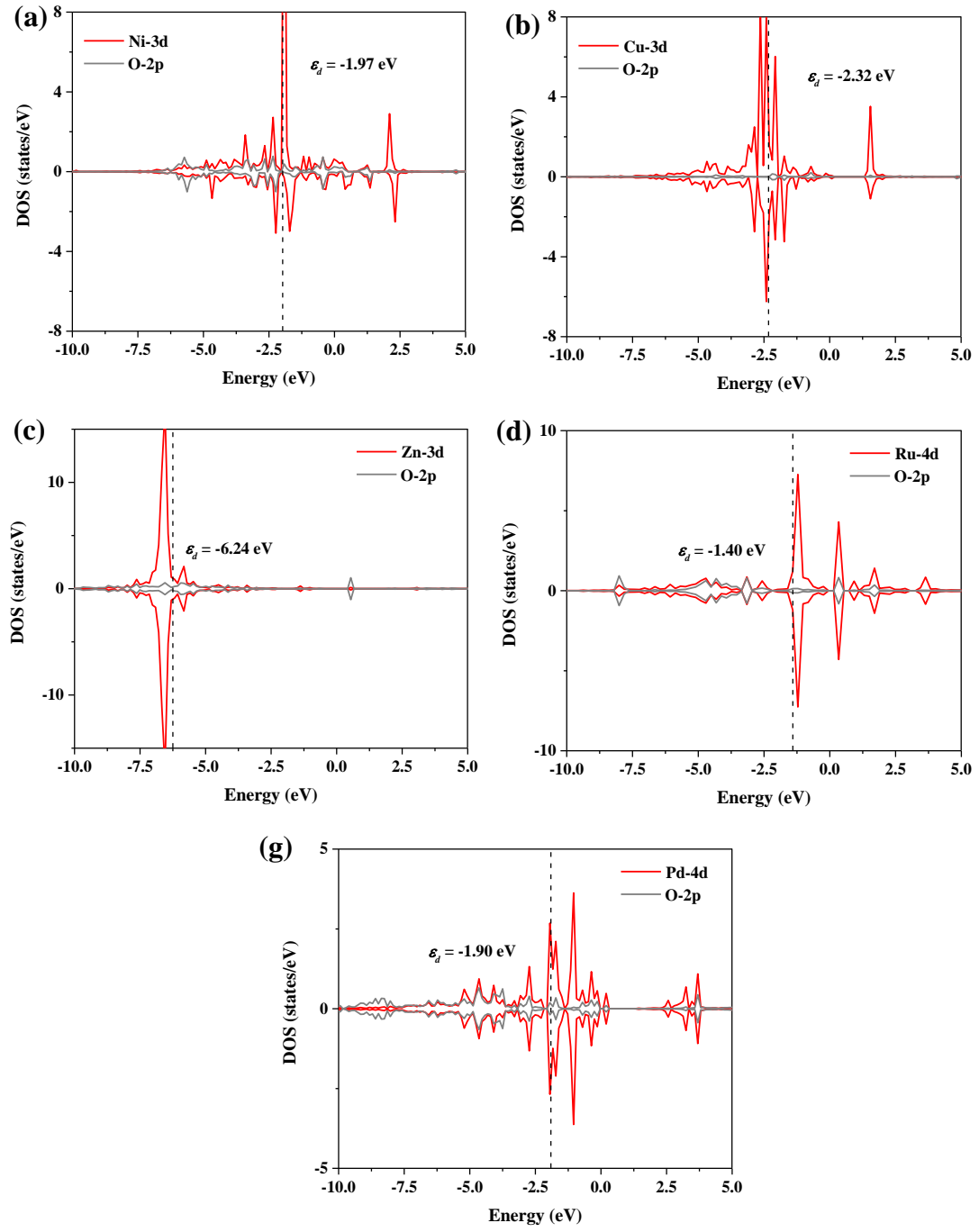


Figure 14. Projected DOS curves for the d orbitals of metal atoms and the 2p orbitals of oxygen atoms in  $\text{OH}^*$ . The Fermi level is 0 eV and the center of the d-band ( $\varepsilon_d$ ) is marked by the dashed line. (a) Ni-SACs@h-BCN, (b) Cu-SACs@h-BCN, (c) Zn-SACs@h-BCN, (d) Ru-SACs@h-BCN, (e) Pd-SACs@h-BCN.

### 3. Tables

Table S1. Optimized lattice parameters of h-BCN monolayer.

Structure	$a$ (Å)	$b$ (Å)
BCN-V1	15.12	8.73
BCN-V2	15.13	15.13
BCN-V3	15.19	8.65

Table S2. Relative Energy ( $\Delta E$ ) and Relative formation energies ( $\Delta E_f$ ) of different Co-SACs@h-BCN structures compared with the Co-SACs@h-BCN-8.

Vacancy Site	Energy (eV)	$\Delta E_f$ (eV)
Co-SACs@h-BCN-1	-2.00	1.02
Co-SACs@h-BCN-2	-2.00	1.02
Co-SACs@h-BCN-3	-2.00	1.02
Co-SACs@h-BCN-4	-2.00	1.02
Co-SACs@h-BCN-5	-2.00	1.02
Co-SACs@h-BCN-6	0.19	4.12
Co-SACs@h-BCN-7	2.03	2.93
Co-SACs@h-BCN-8	0.00	0.00

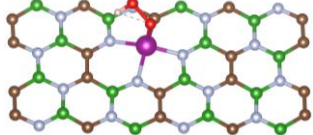
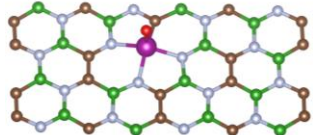
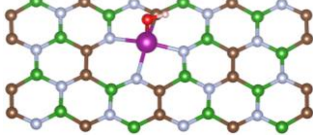
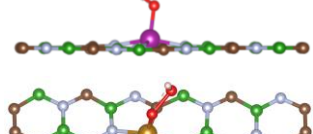
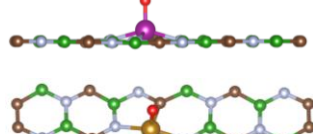
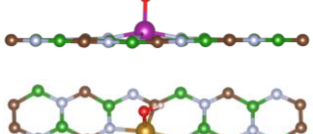
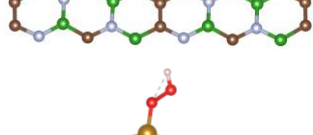
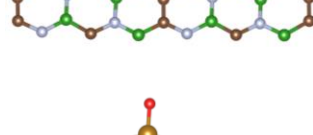
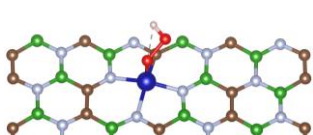
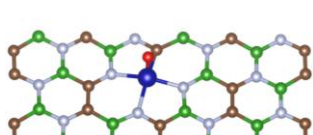
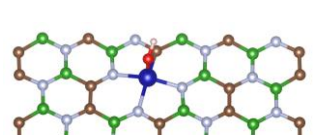
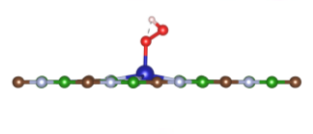
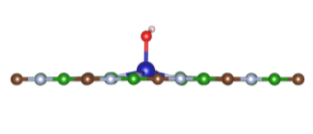
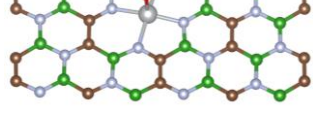
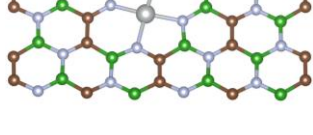
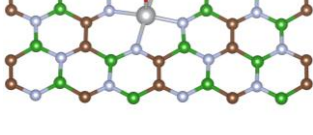
Table S3. Optimized lattice parameters of M-SACs@h-BCN monolayer.

Metal	$a_0$ (Å)	$b_0$ (Å)
Mn	15.16	8.72
Fe	15.14	8.70
Co	15.12	8.70
Ni	15.11	8.69
Cu	15.12	8.69
Zn	15.18	8.70
Ru	15.21	8.70
Rh	15.19	8.70
Pd	15.19	8.70
Ir	15.18	8.70
Pt	15.17	8.75

Table S4. Energies contributed by the entropy ( $TS$ ) and zero-point energy ( $E_{ZPE}$ ) corrections of the free molecules and intermediate species adsorbed on catalysts. All  $E_{ZPE}$  of adsorbates take the value of Fe-N<sub>4</sub> active site since they are not sensitive to the metal atom.

Species	$TS$ (eV)	$E_{ZPE}$ (eV)
OOH*	0	0.42
O*	0	0.07
OH*	0	0.33
H <sub>2</sub> (g)	0.41	0.27
H <sub>2</sub> O (g)	0.67	0.59

Table S5. Optimized structures of different ORR and OER intermediate species on the M-N<sub>3</sub> active site.

Active site	OOH*	O*	OH*
Mn-N <sub>3</sub>			
Fe-N <sub>3</sub>			
Co-N <sub>3</sub>			
Ni-N <sub>3</sub>			
Cu-N <sub>3</sub>			
Zn-N <sub>3</sub>			

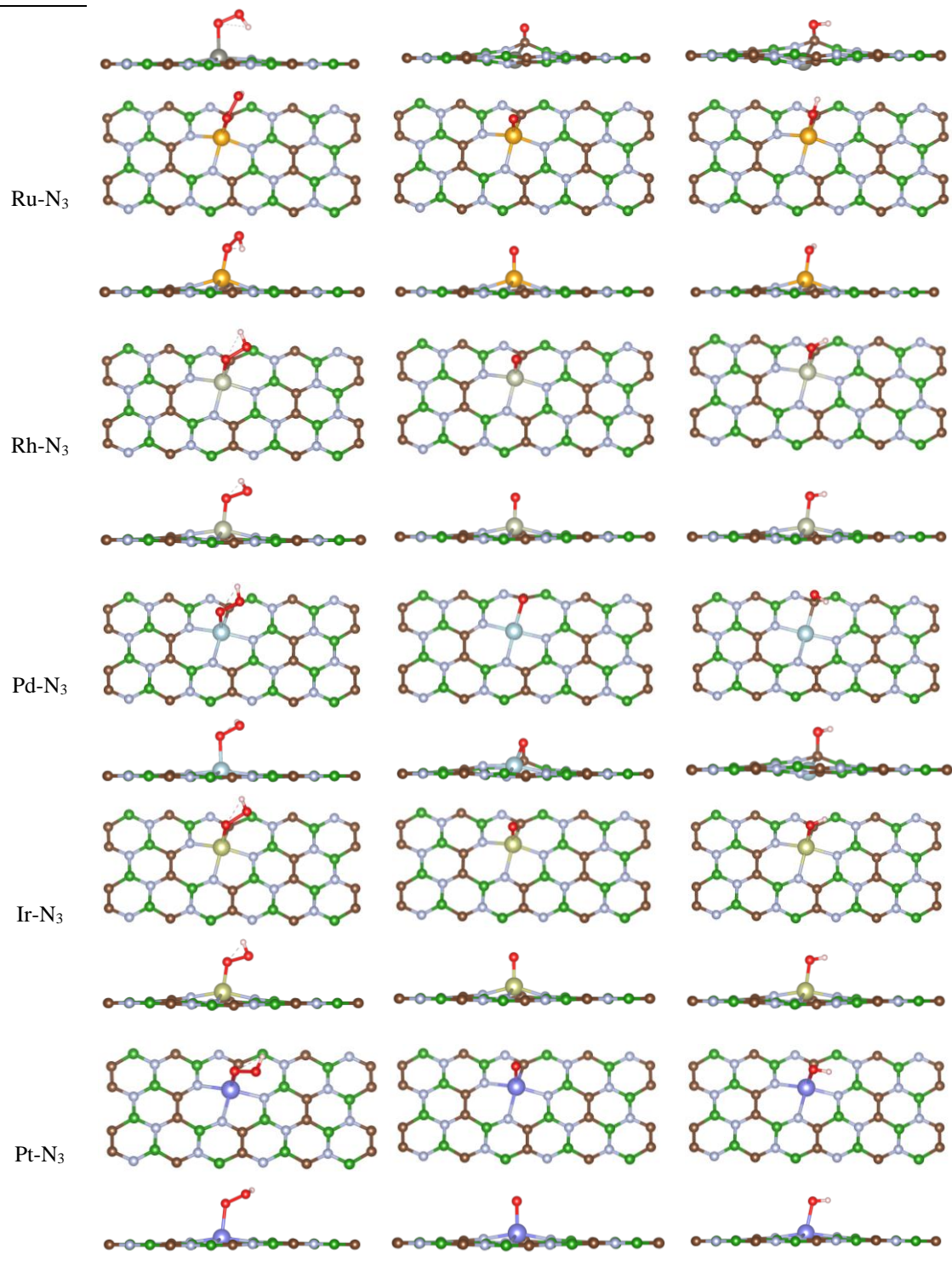


Table S6. The linear relationship formula between the adsorption free energies of oxygen-containing intermediates.

Structure	$\Delta G_{\text{OOH}^*}$	$\Delta G_{\text{O}^*}$	References
h-BCN	$\Delta G_{\text{OOH}^*}=0.98\Delta G_{\text{OH}^*}+3.07$	$\Delta G_{\text{O}^*}=1.46\Delta G_{\text{OH}^*}+0.54$	-
graphene	$\Delta G_{\text{OOH}^*}=0.92\Delta G_{\text{OH}^*}+3.14$	$\Delta G_{\text{O}^*}=1.87\Delta G_{\text{OH}^*}+0.22$	[S5]
$\text{BC}_3$	$\Delta G_{\text{OOH}^*}=0.84\Delta G_{\text{OH}^*}+3.25$	$\Delta G_{\text{O}^*}=1.55\Delta G_{\text{OH}^*}+0.68$	[S6]
$\text{C}_3\text{N}$	$\Delta G_{\text{OOH}^*}=0.86\Delta G_{\text{OH}^*}+3.13$	-	[S7]
Mn-N <sub>x</sub> doped graphene	$\Delta G_{\text{OOH}^*}=0.92\Delta G_{\text{OH}^*}+3.12$	$\Delta G_{\text{O}^*}=0.80\Delta G_{\text{OH}^*}+1.27$	[S8]
cobalt-iron doped graphene	$\Delta G_{\text{OOH}^*}=0.88\Delta G_{\text{OH}^*}+3.09$	$\Delta G_{\text{O}^*}=1.21\Delta G_{\text{OH}^*}+0.47$	[S9]
g-C <sub>4</sub> N <sub>3</sub>	$\Delta G_{\text{OOH}^*}=0.85\Delta G_{\text{OH}^*}+3.09$	$\Delta G_{\text{O}^*}=2.03\Delta G_{\text{OH}^*}+1.02$	[S10]

Table S7. Reaction free energies versus RHE of elementary steps for ORR and OER at  $U=0$  V.

Activate site	ORR (eV)				OER (eV)			
	$\Delta G_1$	$\Delta G_2$	$\Delta G_3$	$\Delta G_4$	$\Delta G_5$	$\Delta G_6$	$\Delta G_7$	$\Delta G_8$
Mn-N <sub>3</sub>	-1.01	-2.64	-0.52	-0.75	0.75	0.52	2.64	1.01
Fe-N <sub>3</sub>	-0.89	-2.35	-0.75	-0.92	0.92	0.75	2.35	0.89
Co-N <sub>3</sub>	-0.84	-1.92	-1.08	-1.08	1.08	1.08	1.92	0.84
Ni-N <sub>3</sub>	-0.03	-4.16	1.19	-1.91	1.91	-1.19	4.16	0.03
Cu-N <sub>3</sub>	0.28	-4.17	-0.33	-0.71	0.71	0.33	4.17	-0.28
Zn-N <sub>3</sub>	-0.16	-5.14	0.10	0.29	-0.29	-0.10	5.14	0.16
Ru-N <sub>3</sub>	-2.56	-2.77	-0.29	0.71	-0.71	0.29	2.77	2.56
Rh-N <sub>3</sub>	-1.38	-1.84	-1.20	-0.49	0.49	1.20	1.84	1.38
Pd-N <sub>3</sub>	0.16	-4.34	0.29	-1.03	1.03	-0.29	4.34	-0.16
Ir-N <sub>3</sub>	-1.28	-2.41	-0.62	-0.61	0.61	0.62	2.41	1.28
Pt-N <sub>3</sub>	0.23	-1.42	-1.65	-2.07	2.07	1.65	1.42	-0.23

Table S8. The potential-determining steps of ORR and OER on the M-N<sub>x</sub> active site.

Active site	ORR	OER
Mn-N <sub>3</sub>	protonation of O* to OH*	hydroxylation of O* to OOH*
Fe-N <sub>3</sub>	protonation of O* to OH*	hydroxylation of O* to OOH*
Co-N <sub>3</sub>	protonation of O <sub>2</sub> to OOH*	hydroxylation of O* to OOH*
Ni-N <sub>3</sub>	protonation of O* to OH*	hydroxylation of O* to OOH*
Cu-N <sub>3</sub>	protonation of O <sub>2</sub> to OOH*	hydroxylation of O* to OOH*
Zn-N <sub>3</sub>	desorption of OH* to OH <sup>-</sup>	hydroxylation of O* to OOH*
Ru-N <sub>3</sub>	desorption of OH* to OH <sup>-</sup>	hydroxylation of O* to OOH*
Rh-N <sub>3</sub>	desorption of OH* to OH <sup>-</sup>	hydroxylation of O* to OOH*
Pd-N <sub>3</sub>	protonation of O* to OH*	hydroxylation of O* to OOH*
Ir-N <sub>3</sub>	desorption of OH* to OH <sup>-</sup>	hydroxylation of O* to OOH*
Pt-N <sub>3</sub>	protonation of O <sub>2</sub> to OOH*	adsorption of OH <sup>-</sup> to OH*

Table S9. The overpotentials of M-N<sub>x</sub> embedded h-BCN monolayer and graphene.

Activate site	BCN monolayer		graphene	
	$\eta_{\text{ORR}}$ (V)	$\eta_{\text{OER}}$ (V)	$\eta_{\text{ORR}}$ (V)	$\eta_{\text{OER}}$ (V)
Mn-N <sub>x</sub>	0.71	1.41	0.78	1.47
Fe-N <sub>x</sub>	0.48	1.12	0.58	1.02
Co-N <sub>x</sub>	0.39	0.69	0.48	0.28
Ni-N <sub>x</sub>	2.42	2.94	1.33	0.89
Cu-N <sub>x</sub>	1.51	2.94	2.17	1.83
Zn-N <sub>x</sub>	1.52	3.91	0.52	1.22
Ru-N <sub>x</sub>	1.94	1.54	--	--
Rh-N <sub>x</sub>	0.74	0.61	--	--
Pd-N <sub>x</sub>	1.52	3.11	--	--
Ir-N <sub>x</sub>	0.62	1.18	--	--
Pt-N <sub>x</sub>	1.46	0.84	--	--

Table S10. The number of occupied  $d$  orbital  $\theta_d$  and electronegativity  $\chi$  of different atoms [S2].

Atom	$\theta_d$	$\chi$
C	-	2.55
N	-	3.04
B	-	2.04
O	-	3.44
Mn	5	1.55
Fe	6	1.83
Co	7	1.88
Ni	8	1.92
Cu	9	1.90
Zn	10	1.65
Ru	7	2.28
Rh	8	2.20
Pd	10	2.20
Ir	7	2.20
Pt	9	2.28

Table S11. Atomic charge transfer numbers of Co, O, H atoms for M-SACs@h-BCN monolayer by Bader charge calculations.

Active site	Co	O	H
Mn-N <sub>3</sub>	-1.47	1.10	-0.68
Fe-N <sub>3</sub>	-1.31	1.10	-0.67
Co-N <sub>3</sub>	-1.12	1.10	-0.71
Ni-N <sub>3</sub>	-0.98	1.09	-0.69
Cu-N <sub>3</sub>	-0.83	1.07	-0.66
Zn-N <sub>3</sub>	-1.10	1.48	-1.00
Ru-N <sub>3</sub>	-1.28	1.39	-1.00
Rh-N <sub>3</sub>	1.04	1.02	-0.63
Pd-N <sub>3</sub>	0.62	1.21	-0.73
Ir-N <sub>3</sub>	-1.14	0.97	-0.59
Pt-N <sub>3</sub>	-1.00	0.99	-0.63

## References

- [S1] Kosasang, S., Ma, N., and Wuamprakhon, P., Insight into the effect of intercalated alkaline cations of layered manganese oxides on the oxygen reduction reaction and oxygen evolution reaction. *Chem. Commun.*, 2018, 54, 8575-8578.
- [S2] Wang, Y., Zhou, N., Li, Y., Electrochemical catalytic mechanism of single transition metal atom embedded BC<sub>3</sub> monolayer for oxygen reduction and evolution reactions. *Chem. Eng. J.*, 2021, 425, 130631.
- [S3] Zhang, Y. Y., Pei, Q. X., Liu, H. Y., and Wei, N., Thermal conductivity of a h-BCN monolayer. *Phys. Chem. Chem. Phys.*, 2017, 19, 27326-27331.
- [S4] Beniwal, S., Hooper, J., Miller, D. P., Costa, P. S., Chen, G., Liu, S. Y., Dowben, P. A., Sykes, E. C. H., Zurek E., and Enders, A., Graphene-like boron-carbon-nitrogen monolayers. *ACS Nano*, 2017, 11, 2486-2493.
- [S5] Xu, H., Cheng, D., Cao, D., and Zeng, X. C., A universal principle for a rational design of single-atom electrocatalysts. *Nat. Catal.*, 2018, 1, 339-348.
- [S6] Wang, Y., Zhou, N., and Li, Y., Electrochemical catalytic mechanism of single transition metal atom embedded BC<sub>3</sub> monolayer for oxygen reduction and evolution reactions. *Chem. Eng. J.*, 2021, 425, 130631.
- [S7] Zhou, Y., Gao, G., Kang, J., Chu, W., and Wang, L. W., Transition metal-embedded two-dimensional C<sub>3</sub>N as a highly active electrocatalyst for oxygen evolution and reduction reactions. *J. Mater. Chem. A*, 2019, 7, 12050-12059.
- [S8] Zhu, G., Liu, F., Wang, Y., Wei, Z., and Wang, W., Systematic exploration of N, C coordination effects on the ORR performance of Mn-N<sub>x</sub> doped graphene catalysts based on DFT calculations. *Phys. Chem. Chem. Phys.*, 2019, 21, 12826-12836.
- [S9] Sun, Y., Wang, J., Liu, Q., Xia, M., Tang, Y., Gao, F., Hou, Y., Tse, J., and Zhao, Y. (2019). Itinerant ferromagnetic half metallic cobalt-iron couples: promising bifunctional electrocatalysts for ORR and OER. *J. Mater. Chem. A*, 2019, 7, 27175-27185.
- [S10] Yang, F., Zhu, X., Jia, B., Hao, J., Ma, Y., Lu, P., and Li, D., Trifunctional

electrocatalysts of single transition metal atom doped g-C<sub>4</sub>N<sub>3</sub> with high performance for OER, ORR and HER. Inter. J. Hydro. Energy, 2024, 51, 195-206.